Preprints of the 21st IFAC World Congress (Virtual)
Berlin, Germany, July 12-17, 2020

Automatic Deep Stall Recovery using Optimal Trajectory Planning

MLD Babl * **JAA Engelbrecht** *

* *Stellenbosch University (e-mail: 18964702@sun.ac.za; jengelbr@sun.ac.za)*

Abstract: This paper presents the design of an automatic deep stall recovery algorithm for large transport aircraft using optimal trajectory planning. Deep stall is a condition where an aircraft is trapped in a nose-high stall condition and its elevators cannot produce enough nose-down pitching moment to recover the aircraft from the stall. The NASA Generic Transport Model (GTM) is used as the basis for the design and verification of the system. The aerodynamic model of the NASA GTM simulation model is modified to exhibit deep stall behaviour. Simulations are performed to show that the modified aircraft model can be pushed into deep stall, and cannot be recovered using elevator actions only. The deep stall recovery task is formulated as an optimal path planning problem and solved using an A^* search algorithm to find the optimal sequence of control actions and the resulting optimal state trajectory to escape from the deep stall. The A^* algorithm performs the planning using a simplified, three-degrees-of-freedom (3DOF) aircraft model that models only the fast rotational dynamics. The automatic deep stall recovery is then verified in simulation using the full six-degrees-of-freedom (6DOF) NASA GTM aircraft model. The simulation results show that the system successfully recovers the aircraft from deep stall. The optimal sequence of control actions first uses the rudder to yaw the horizontal tailplane out of the aircraft's own wake to regain elevator effectiveness, and then uses the elevators to pitch the nose down and recover from the stall.

Keywords: Autonomous Vehicles, Safety, Trajectory Planning, Transportation, Tree Searches

1. INTRODUCTION

Despite the fact that envelope protection functions are implemented on modern commercial aircraft, situations still arise where the aircraft exits the flight envelope due to environmental factors, pilot error, or component failures. Since the envelope protection functions are only designed to prevent the aircraft from exiting the flight envelope, and not to recover the aircraft to its flight envelope after a departure, the envelope recovery procedure must be performed manually by the pilot. A need therefore exists for flight envelope recovery functions that assist the pilot in recovering the aircraft to its flight envelope after a severe upset.

This paper focusses on the problem of automatic deep stall recovery. Deep stall is a condition where an aircraft is trapped in a nose-high stall condition and its elevators cannot produce enough nose-down pitching moment to recover the aircraft from the stall (Chambers and Grafton, 1977). Deep stall is most often exhibited by aircraft with high horizontal tailplanes, such as T-tail transport aircraft and jet fighter aircraft with high horizontal tails. At very high angles of attack the horizontal tail is immersed in the combined wake of the wings, engines and fuselage. The effect is to produce a nonlinear variation of pitching moment as a function of angle of attack, resulting in two ranges of stable trim points, the normal range at low angle of attack, and a deep stall range at high angle of attack. In deep stall, the effectiveness of the elevators is also significantly decreased due to the low-energy wake impinging on the horizontal tailplane, leaving insufficient nose-down pitching moment to recover from the deep stall trim point.

The appropriate deep stall recovery procedure is dependent on the specific aircraft configuration (Medina and Shahaf, 1990). One possible strategy to escape from deep stall is to yaw the horizontal tailplane out of the wake using the rudder to regain elevator effectiveness, and then to use the elevators to recover from the stall. Another possible strategy, called the "pitch rocking" method, is to pitch the aircraft up and down at a specific resonant frequency, to build up the amplitude of the pitch angle oscillations until the angle of attack escapes the deep stall.

We propose an automatic deep stall recovery algorithm that finds the correct deep stall recovery sequence for the specific aircraft using a model of its flight dynamics. We formulate the deep stall recovery task is a constrained optimal path planning problem and then solve the problem using an A^* search algorithm to find the optimal sequence of control actions and the resulting optimal state trajectory to escape from the deep stall.

2. RELATED WORK

Several studies have been performed on stall and spin recovery for fighter aircraft. Kumar et al. (2004) used bifurcation techniques together with nonlinear dynamic inversion for spin prediction and recovery of a fighter aircraft. Lee and Nagati (2004) presented a momentum vector

control law for spin recovery. Raghavendra et al. (2005) presented a spin recovery control law, with and without thrust vectoring, using nonlinear dynamic inversion. Dutoi et al. (2008) presented a spin recovery system that combines robust control and reinforcement learning. Sinha and Venkateswara Rao (2010) presented a sliding-mode controller for spin recovery based on a variable-structure control technique. Yildiz et al. (2018) developed a finite state automata based approach to autonomous stall and upset recovery for agile aircraft.

Several recent studies have been performed on stall and spin recovery for large transport aircraft and general aviation aircraft. Engelbrecht et al. performed a bifurcation analysis of the nonlinear dynamics of a large transport aircraft to show how the natural stability of the aircraft could be used for stall and spin recovery (Engelbrecht et al., 2012; Pauck and Engelbrecht, 2012). Gill et al. presented the use of bifurcation analysis, complemented by time-history simulations, to characterise spiral and spin behaviour of the NASA generic transport model in upset conditions, in both open-loop and closed-loop configurations (Gill et al., 2013, 2015). Engelbrecht (2016) proposed two flight envelope recovery approaches for large transport aircraft. The first approach uses a passive method to recover the aerodynamic envelope using the natural stability of the aircraft and then uses the conventional flight control laws, with their flight envelope protection functions, to recover the aircraft attitude and flight vector (Engelbrecht et al., 2013). The second approach uses an active method to recover the aerodynamic envelope using a Lyapunov-based inner-loop controller and uses an outer-loop controller based on optimal control theory to recover the aircraft attitude, flight path angle and airspeed while minimising the altitude loss. Bunge and Kroo (2018) presented a spin recovery system for general aviation aircraft that consists of a spin arrest controller and an optimal pullout controller that minimises the altitude loss.

Only a few studies have addressed the problem of automatic deep stall recovery. Hahn et al. (2007) presented the design and validation of an automatic pitch rocker system to perform deep stall recovery for a fighter aircraft. Wang and Shi (2010) designed a fuzzy controller for deep stall recovery based on particle swarm optimization.

Our literature review therefore reveals that automatic deep stall recovery has not been adequately covered by previous research. We therefore present an automatic deep stall recovery algorithm for large transport aircraft using optimal trajectory planning. We will pose the deep stall recovery problem as an optimal control task, and we will solve it using an A^* search algorithm.

3. AIRCRAFT MODEL

The NASA Generic Transport Model (GTM), shown in Fig. 1, is used as the basis for the design and verification of the automatic deep stall recovery system. The NASA GTM is a 5.5% dynamically scaled unmanned aerial vehicle (UAV) of a large transport aircraft that was developed by NASA for experimental flight tests outside the normal flight envelope. Wide-envelope aerodynamic models were developed for the NASA GTM based on wind tunnel tests over an extensive range of angles of attack, sideslip angles, angular rates, and control surface deflections (Foster et al., 2005; Murch and Foster, 2007; Murphy and Klein, 2008; Cunningham et al., 2008). A full nonlinear simulation model of the GTM was created and made available by NASA for passenger aircraft upset recovery research (Hueschen, 2011).

Fig. 1. The NASA Generic Transport Model

For this paper, the aerodynamic model of the NASA GTM simulation model was modified to exhibit deep stall behaviour. The aerodynamic forces and moments acting on the aircraft are calculated using a set of non-dimensional aerodynamic coefficient functions C_X, C_Y, C_Z, C_l, C_m, and C_n. The non-dimensional aerodynamic coefficients are nonlinear, multivariate functions and are implemented as multi-dimensional lookup tables with contributions from static forces and moments due to angle of attack and sideslip angle, dynamic forces and moments due to the body angular rates, and control surface forces and moments due to the deflections of the ailerons, elevator, and rudder. The following set of functions were developed by Murch (2007) to model the non-dimensional aerodynamic coefficients of the unmodified NASA GTM

$$\begin{aligned} C_X =& C_{X,static}(\alpha,\beta) + \Delta C_{X,\delta}(\alpha,\beta,\delta_E,\delta_A,\delta_R) \\ &+ \Delta C_{X,\hat{q}_{osc}}(\alpha,\hat{q}_{osc}) + \Delta C_{X,\hat{\omega}_{ss}}(\alpha,\beta,\hat{\omega}_{ss}) \end{aligned} \tag{1}$$

$$\begin{aligned} C_Y =& C_{Y,static}(\alpha,\beta) + \Delta C_{Y,\delta}(\alpha,\beta,\delta_A,\delta_R) \\ &+ \Delta C_{Y,\hat{p}_{osc}}(\alpha,\hat{p}_{osc}) + \Delta C_{Y,\hat{r}_{osc}}(\alpha,\hat{r}_{osc}) \\ &+ \Delta C_{Y,\hat{\omega}_{ss}}(\alpha,\beta,\hat{\omega}_{ss}) \end{aligned} \tag{2}$$

$$\begin{aligned} C_Z =& C_{Z,static}(\alpha,\beta) + \Delta C_{Z,\delta}(\alpha,\beta,\delta_E,\delta_A,\delta_R) \\ &+ \Delta C_{Z,\hat{q}_{osc}}(\alpha,\hat{q}_{osc}) + \Delta C_{Z,\hat{\omega}_{ss}}(\alpha,\beta,\hat{\omega}_{ss}) \end{aligned} \tag{3}$$

$$\begin{aligned} C_l =& C_{l,static}(\alpha,\beta) + \Delta C_{l,\delta}(\alpha,\beta,\delta_A,\delta_R) \\ &+ \Delta C_{l,\hat{p}_{osc}}(\alpha,\hat{p}_{osc}) + \Delta C_{l,\hat{r}_{osc}}(\alpha,\hat{r}_{osc}) \\ &+ \Delta C_{l,\hat{\omega}_{ss}}(\alpha,\beta,\hat{\omega}_{ss}) \end{aligned} \tag{4}$$

$$\begin{aligned} C_m =& C_{m,static}(\alpha,\beta) + \Delta C_{m,\delta}(\alpha,\beta,\delta_E,\delta_A,\delta_R) \\ &+ \Delta C_{m,\hat{q}_{osc}}(\alpha,\hat{q}_{osc}) + \Delta C_{m,\hat{\omega}_{ss}}(\alpha,\beta,\hat{\omega}_{ss}) \end{aligned} \tag{5}$$

$$\begin{aligned} C_n =& C_{n,static}(\alpha,\beta) + \Delta C_{n,\delta}(\alpha,\beta,\delta_A,\delta_R) \\ &+ \Delta C_{n,\hat{p}_{osc}}(\alpha,\hat{p}_{osc}) + \Delta C_{n,\hat{r}_{osc}}(\alpha,\hat{r}_{osc}) \\ &+ \Delta C_{n,\hat{\omega}_{ss}}(\alpha,\beta,\hat{\omega}_{ss}) \end{aligned} \tag{6}$$

The NASA GTM's aerodynamic model was modified to exhibit deep stall behaviour by modifying the static pitching moment coefficient $C_{m,\text{static}}(\alpha,\beta)$ with respect to angle of attack and sideslip angle, and the incremental pitching moment coefficient with respect to elevator deflection

$\Delta C_{m,\delta}(\alpha, \beta, \ldots, \delta_E)$. The static pitching moment coefficient was modified as shown in Fig. 2 to have three equilibrium points at angles of attack of 6, 20, and 28 degrees, where $C_{m,\text{static}}$ is zero for the same elevator deflection.

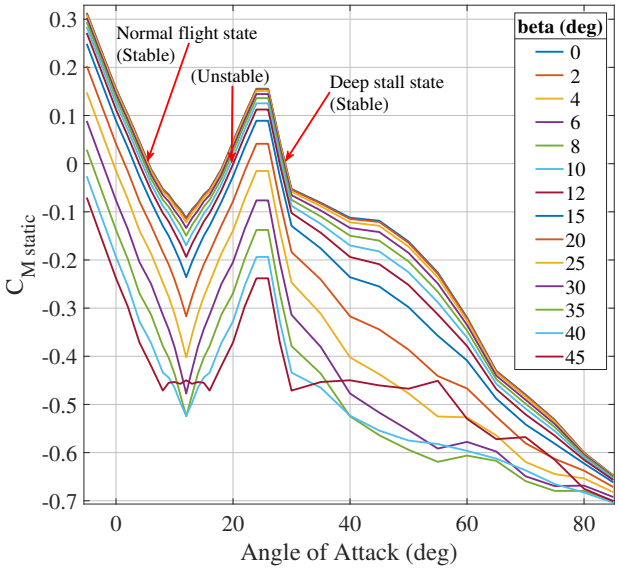

Fig. 2. The NASA GTM static pitching moment coefficient with respect to angle of attack and sideslip angle, modified to have a stable deep stall state.

The first equilibrium point at $\alpha = 6$ degrees is stable and represents the normal flight state. The third equilibrium point at $\alpha = 28$ degrees is also stable, but represents the deep stall state. The second equilibrium point at $\alpha = 20$ degrees is unstable, and any perturbations from the state will result in the aircraft state moving to either the normal flight state or the deep stall state. A positive pitching moment causes an increase in the angle of attack and a negative pitching moment causes a decrease in angle of attack. Angles of attack above 20 degrees have a positive pitching moment until the deep stall equilibrium angle of attack where after it becomes negative. Therefore any deviation from a stable equilibrium will result in a pitching moment which will drive the system back towards the equilibrium. The modification to $C_{m,\text{static}}$ causes the aircraft to be attracted to the deep stall state at angles past 20 degrees.

The incremental pitching moment coefficient with respect to elevator deflection was modified as shown in Fig. 3 so that the elevator loses pitching moment effectiveness at angles of attack $\alpha > 11$ degrees and sideslip angles $\beta < 2$ degrees. Note that the ailerons and rudder do not lose their effectiveness in deep stall. The modification to $\Delta C_{m,\delta}(\alpha, \beta, \ldots, \delta_E)$ represents the fact that the elevators lose effectiveness when they are in the aircraft's wake at high angles of attack, but regain effectiveness when the sideslip angle is increased to swing the tail out of the wake.

Finally, the original NASA GTM aerodynamic model was modified to remove non-zero rolling and yawing moments that are present at high angles of attack and zero sideslip angle, to prevent the aircraft from naturally departing from the deep stall condition.

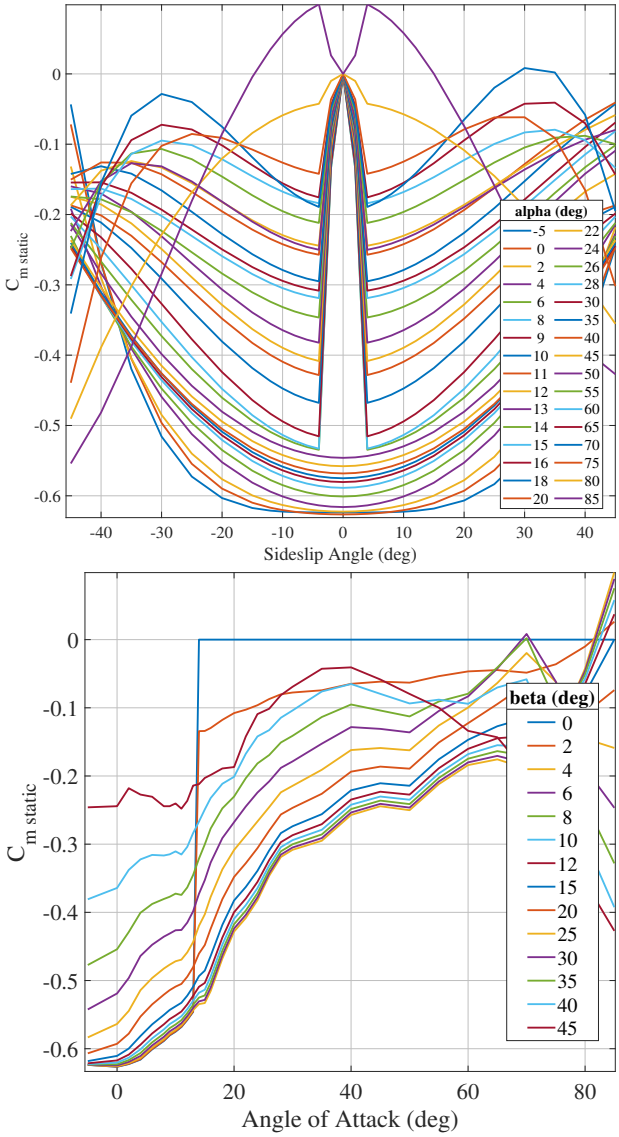

Fig. 3. The NASA GTM incremental pitching moment coefficient with respect to elevator, modified to lose effectiveness in the aircraft's wake.

A simulation was performed to show that the modified NASA GTM model can be pushed into deep stall, and cannot be recovered by elevator actions only. The simulation results are shown in Fig. 4 and 5. The time histories of the angle of attack, sideslip angle, aileron, elevator, and rudder are shown in Fig. 4. The aircraft starts the simulation in normal flight with an angle of attack of $\alpha = 6$ degrees and all the control surfaces set to their trim deflections. At $t = 1$ second, a nose-up elevator deflection of $\delta_E = 30$ degree is commanded, and the aircraft is pushed into deep stall. The angle of attack increases from 6 to 30 degrees, while the sideslip angle remains near zero. At $t = 2$ seconds, the elevator is returned to its trim deflection, but the aircraft remains at a high angle of attack. A transient is observed in the angle of attack due to the flight path angle decreasing because of the loss of lift in deep stall. Eventually, the angle of attack settles at the stable deep stall angle of attack of $\alpha = 28$ degrees. After $t = 10$ seconds, an attempt is made to recover the aircraft from deep stall using elevator action only. A nose-down elevator

deflection of +20 degrees is commanded, but due to the loss of elevator effectiveness, the aircraft remains trapped in deep stall. Fig. 5 shows the aircraft's trajectory for the simulated deep stall entry and attempted recovery. The aircraft enters deep stall and then continues to enter a spiral motion.

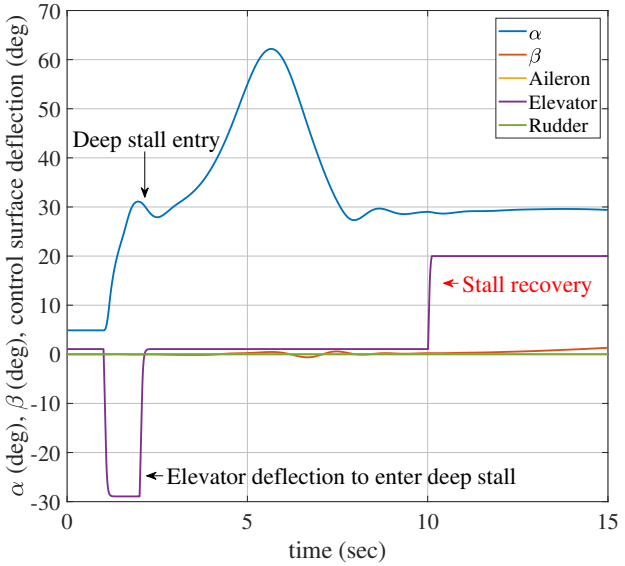

Fig. 4. The time histories of a simulated deep stall entry and attempted recovery using elevator.

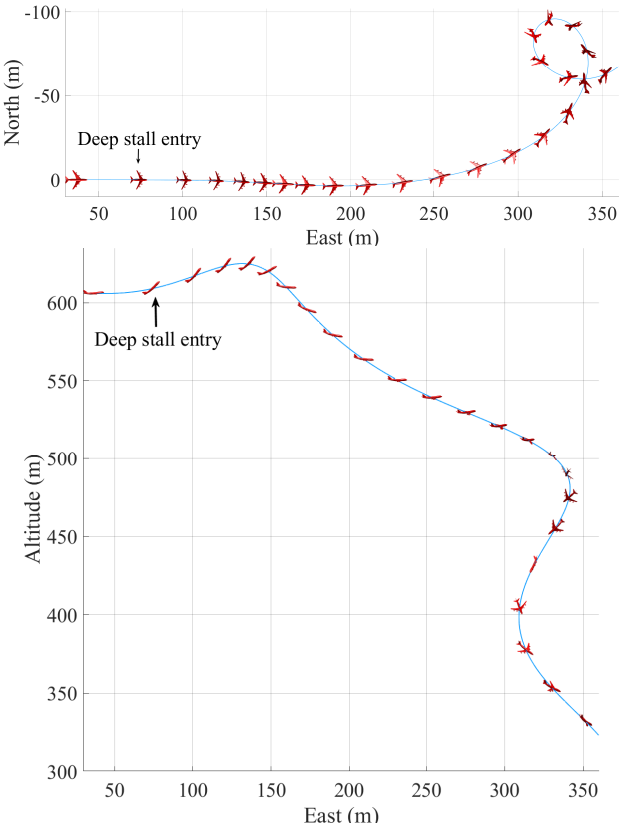

Fig. 5. The aircraft's trajectory (top view and side view) for the simulated deep stall entry and attempted recovery using elevator only.

4. DEEP STALL RECOVERY SYSTEM

4.1 System Overview

The architecture of our proposed deep stall recovery system is shown in Fig. 6.

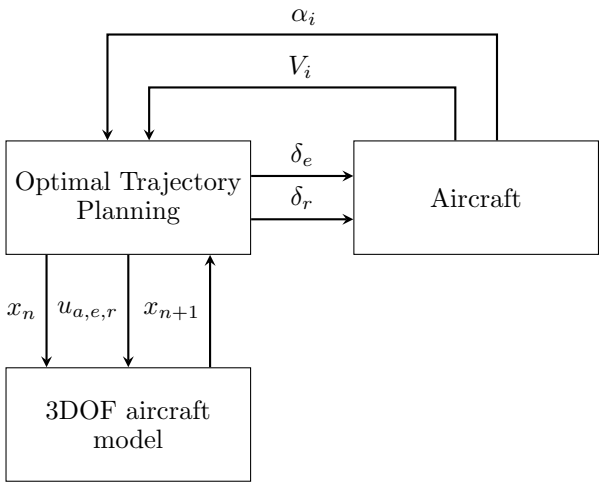

Fig. 6. The architecture of the deep stall recovery system.

Once the system detects that the aircraft is in a deep stall condition, it uses a reduced-order, three-degrees-of-freedom (3DOF) model of the aircraft's fast rotational dynamics to determine the sequence of elevator and rudder actions that will transition the aircraft from its initial state in the deep stall region to a final state in the normal flight region. (The 3DOF model is sufficient for planning because the stall recovery is primarily a rotational recovery.) The deep stall recovery task is formulated as an optimal control problem and is solved using an A^* trajectory planning algorithm. The optimal sequence of elevator and rudder actions are then applied to the real aircraft to perform the deep stall recovery.

4.2 The Optimal Control Problem

The deep stall recovery task is formulated as an optimal control problem with the objective of finding the optimal sequence of control actions and the resulting optimal state trajectory to escape from the deep stall. The dynamic system is defined as the simplified, third-order nonlinear differential equations describing the fast rotational dynamics of the aircraft, while the slower point mass translational dynamics are treated as quasi-static. The fast rotational dynamics model therefore includes the wide-envelope aerodynamic models describing the aerodynamic moments, but not the aerodynamic forces.

The physical limits on the angle of attack, sideslip angle, and angular rates are specified by defining the sets of admissible states. The physical limits on the elevator and rudder deflections are specified by defining sets of admissible inputs. The requirement to recover the aircraft to the normal aerodynamic envelope (low angle of attack, low sideslip angle, and low angular rates) is translated into a set of admissible final states. The objective to recover the angle of attack as quickly as possible is translated into a

cost function that is the time integral of the sum of the squares of the angle of attack and the sideslip angle.

Note that the deep stall recovery is not concerned with recovering the gross attitude (pitch angle and bank angle) of the aircraft relative to the inertial reference frame, nor is it concerned with recovering the flight vector (flight path angle and airspeed) of the aircraft. The purpose of deep stall recovery is rather to recover the angle of attack, sideslip angle and angular rates of the aircraft to the normal aerodynamic envelope where the normal flight control laws can be used to recover the gross attitude and point mass translation motion.

Problem Formulation: Given the initial state of the aircraft in the deep stall region (high angle of attack, low sideslip angle), the objective is to find the optimal sequence of elevator and rudder actions that will transition the aircraft to a final state in the normal flight region (low angle of attack, low sideslip angle) as quickly as possible, while obeying the aircraft's aerodynamic and physical constraints.

Dynamic System: The dynamic system is represented by the reduced-order, three-degrees-of-freedom nonlinear differential equations that describe the fast rotational dynamics of the aircraft.

The rotational kinematics that relates the angle of attack α and the sideslip angle β to the angular rates P, Q, and R is given by

$$\begin{bmatrix}\dot{\alpha}\\ \dot{\beta}\end{bmatrix} = \begin{bmatrix}-\cos\alpha\tan\beta & 1 & -\sin\alpha\tan\beta\\ \sin\alpha & 0 & -\cos\alpha\end{bmatrix}\begin{bmatrix}P\\ Q\\ R\end{bmatrix} \tag{7}$$

The rotational dynamics that relates the angular acceleration of the aircraft to the aerodynamics moments acting on the aircraft body is given by

$$\begin{bmatrix}\dot{P}\\ \dot{Q}\\ \dot{R}\end{bmatrix} = \mathbf{I_B}^{-1}\left(-\begin{bmatrix}P\\ Q\\ R\end{bmatrix}\times \mathbf{I_B}\begin{bmatrix}P\\ Q\\ R\end{bmatrix} + \begin{bmatrix}L_A\\ M_A\\ N_A\end{bmatrix}\right) \tag{8}$$

where $\mathbf{I_B}$ is the moment of inertia matrix of the aircraft body, and L_A, M_A, and N_A are the aerodynamic moments acting on the aircraft. The aerodynamic moments are modelled by the following nonlinear equations

$$\begin{bmatrix}L_A\\ M_A\\ N_A\end{bmatrix} = \frac{1}{2}\rho\bar{V}^2 S\begin{bmatrix}bC_l\\ \bar{c}C_m\\ bC_n\end{bmatrix}(\alpha,\beta,P,Q,R,\delta_A,\delta_E,\delta_R) \tag{9}$$

where ρ is the air density, $\bar{V}$ is the airspeed, S, $\bar{c}$, and b are the surface area, mean aerodynamic chord, and span of the wings, C_l, C_m, and C_n are the aerodynamic coefficient functions for rolling moment, pitch moment, and yawing moment, and δ_A, δ_E, and δ_E are the aileron, elevator and rudder deflections.

System state: The state vector $\mathbf{x}$ is defined as

$$\mathbf{x}(t) = [\alpha\ \beta\ P\ Q\ R]^T \tag{10}$$

where α and β are the angle of attack and sideslip angle, P, Q and R are the roll rate, pitch rate and yaw rate coordinated in the body axis system.

Control input: The control input vector $\mathbf{u}$ is defined as

$$\mathbf{u}(t) = [\delta_A\ \delta_E\ \delta_R]^T \tag{11}$$

where δ_A, δ_E, and δ_E are the aileron, elevator and rudder deflections.

State constraints: The state constraints are defined by the range of admissible states over which the aerodynamic model of the NASA GTM is valid.

$$\begin{aligned}\alpha(t) &\in [-5,+60]\\ \beta(t) &\in [-45,+45]\\ P(t) &\in [-200,+200]\\ Q(t) &\in [-80,+80]\\ R(t) &\in [-90,+90]\end{aligned}$$

Input constraints: The control input constraints are defined by the range of admissible aileron, elevator, and rudder deflections

$$\begin{aligned}\delta_A(t) &\in [-30,+30]\\ \delta_E(t) &\in [-30,+20]\\ \delta_R(t) &\in [-45,+45]\end{aligned}$$

Goal Region / Terminal state constraints: The requirement to recover the aircraft to the normal aerodynamic envelope (low angular rates, low angle of attack, and low sideslip angle) is translated into a goal region, or a set of admissible final states

$$\begin{aligned}\alpha(t_f) &\in [-5,+10]\\ \beta(t_f) &\in [-10,+10]\\ P(t_f) &\in [-30,+30]\\ Q(t_f) &\in [-30,+30]\\ R(t_f) &\in [-30,+30]\end{aligned}$$

Cost function: The objective to return the angle of attack to the normal aerodynamic envelope as soon as possible is translated into the following cost function

$$J = \int_{t_0}^{t_f}(\alpha(t)-\alpha_{\text{trim}})^2 + (\beta(t)-\beta_{\text{trim}})^2\,dt \tag{12}$$

where t_0 is the initial time, t_f is the final time, and α_{trim} and β_{trim} are the trim angle of attack and sideslip angle to which the aircraft must be recovered.

4.3 The A Solution*

The optimal control problem is solved using the general A^* algorithm, shown in algorithm 1, described by LaValle (2006). The A^* algorithm was chosen because the five-dimensional state space of the 3DOF rotational dynamics model is too large for the optimal control problem to be solved using dynamic programming. The A^* algorithm starts at the initial state x_I and then generates all possible next states x' by applying all possible actions u. Each new state that was generated is then visited, and their

Algorithm 1 Generic A^* Algorithm

```
Q_open.insert(x_I)
while Q_open not empty and size(Q_closed) < N_max do
    x ← Q_open.getFirst()
    if x == x_G then
        return SUCCESS
    else
        for all u ∈ U do
            x' ← f(x, u)
            if x' valid then
                Q_open.insert(x')
        Q_closed.insert(x)
return FAILURE
```

next states are generated by applying all possible actions again. The process is then iterated to grow a search tree until a goal state is found. Once a goal state is found, the algorithm follows the trail of previous states to determine the path from the initial state to the goal state. To find the optimal path, the A^* algorithm sorts the new states that are generated in a priority queue Q_{open} from the lowest path cost to the highest path cost. The total path cost of a given state is calculated by adding the cost to come (the cost to reach the given state from the initial state) and the cost to go (the cost to reach the goal state from the given state). The cost to go is estimated using a heuristic function. By visiting the lowest cost states first, the A^* algorithm ensures that the first path that is found, will also be the optimal path.

Algorithm Execution: A search tree is created to determine the optimal trajectory for the deep stall recovery. Each node in the tree contains the state, the action, the cost, and the time index of a possible point along the recovery trajectory. Starting from the aircraft's initial state in the deep stall region, the search tree is grown to try and reach the goal region. For each node that is already in the tree, the discrete-time, reduced-order, three-degrees-of-freedom model of the aircraft's fast rotational dynamics is used to generate new child nodes using all combinations of available elevator and rudder actions in the action space. A priority queue is used to determine the order in which nodes are expanded. When a new child node is created, its state is checked to make sure that it is admissible before it is added to the priority queue. The nodes in the priority queue are ordered from lowest to highest cost, so that the nodes with the lowest cost are expanded first. The A^* algorithm terminates when the goal set is reached, or when the open queue is empty, or when the algorithm exceeds a predefined maximum number of iterations.

State transition equation: The following discrete-time, reduced-order, three-degrees-of-freedom model of the aircraft's fast rotational dynamics is used as the state transition equation to generate the child nodes from a given parent node

$$\begin{aligned}
\alpha(k+1) &= \alpha(k) + \dot{\alpha}(k)\Delta T \\
\beta(k+1) &= \beta(k) + \dot{\beta}(k)\Delta T \\
P(k+1) &= P(k) + \dot{P}(k)\Delta T \\
Q(k+1) &= Q(k) + \dot{Q}(k)\Delta T \\
R(k+1) &= R(k) + \dot{R}(k)\Delta T
\end{aligned} \tag{13}$$

where k is the time index of the parent node, $k+1$ is the time index of the child node, ΔT is the sampling period of the discrete time step. The time derivatives $\dot{\alpha}$, $\dot{\beta}$, $\dot{P}$, $\dot{Q}$, and $\dot{R}$ for a given set of inputs δ_A, δ_E, and δ_R are calculated using equations 7, 8, and 9.

Action space: The following discrete action space, consisting of a finite set of available elevator and rudder actions, is used to generate the child nodes from a given parent node

$$\begin{aligned}
\delta_A(k) &\in \{0\} \\
\delta_E(k) &\in \{-30, -20, -10, 0, +6.667, +13.333, +20\} \\
\delta_R(k) &\in \{-45, -30, -15, 0, +15, +30, +45\}
\end{aligned}$$

It is assumed that the ailerons will not be used for the deep stall recovery.

Cost to come: The cost to come for each node is calculated incrementally as nodes are created and added to the search tree. The cost to come is the discrete-time integral of the sum of the squares of the angle of attack and the sideslip angle. The cost to come of a child node is calculated as the sum of the cost to come of the parent node and the incremental cost to transition from the parent node to the child node.

$$G(k+1) = G(k) + \Delta G \tag{14}$$

with

$$\Delta G = (\alpha(k+1) - \alpha(k))^2 + (\beta(k+1) - \beta(k))^2 \Delta T \tag{15}$$

where $G(k)$ is the cost to come of the parent node, $G(k+1)$ is the cost to come of the child node, and ΔG is the incremental state transition cost.

Cost to go heuristic: The cost to go for each node is calculated using a heuristic function that estimates the cost of the cheapest path from the child node to a goal node.

$$H(k+1) = (\alpha(k+1) - \alpha_{\text{trim}})^2 + (\beta(k+1) - \beta_{\text{trim}})^2 \tag{16}$$

The cost to go is estimated to be the sum of the squares of the difference between the angle of attack and sideslip angle at the child node, and the angle of attack and the sideslip angle at trim.

Total path cost: The total path cost for each node is the sum of its cost to come and its cost to go.

$$J(k) = G(k) + H(k) \tag{17}$$

where J is the total path cost, G is the cost to come, and H is the cost to go for a given node in the deep stall recovery trajectory.

4.4 Optimal Trajectory Planning

The optimal trajectory planner was used to find the sequence of control actions and the associated state trajectory to recover the aircraft from a given initial state in the deep stall region. The planned sequence of control inputs and their expected deep stall recovery trajectory are shown in Fig. 7. (Remember that the planned state trajectory and input sequence are generated using the simplified 3DOF aircraft model.) The initial deep stall

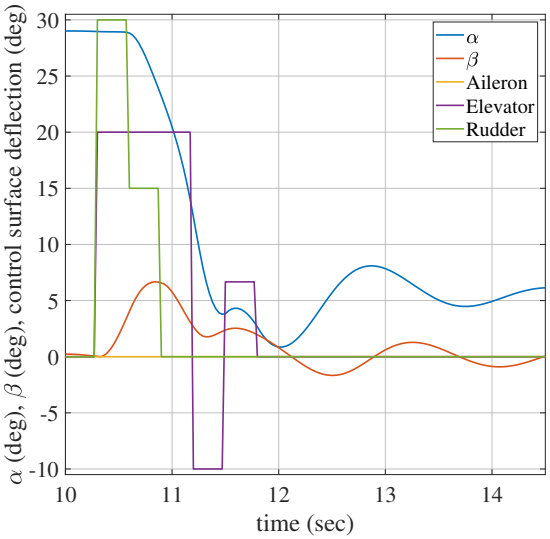

Fig. 7. Planned deep stall recovery actions and trajectory.

state that was given to the optimal trajectory planner was obtained from the deep stall simulation performed with the full 6DOF GTM model in section 3. The state at time $t = 10$ seconds in Fig. 4, when the aircraft had already settled at the deep stall angle of attack, was assumed to be the initial deep stall state from which the aircraft must be recovered. The time histories in Fig. 7 show that the intial state of the aircraft at $t = 10$ seconds is an angle of attack of $\alpha = 28$ degrees and a sideslip angle of $\beta = 0$ degrees. The planned sequence of recovery actions starts by simultaneously applying a rudder deflection $\delta_R = 30$ degrees and a nose-down elevator deflection $\delta_E = 20$ degrees. The rudder deflection causes the sideslip angle β to increase from 0 to 6 degrees, effectively swinging the horizontal tailplane out of the aircraft's wake to regain elevator effectiveness. When the sideslip angle β exceeds about 5 degrees, the angle of attack α starts recovering due to the nose-down pitching moment produced by the elevators. While the angle of attack recovers, the rudder deflection is reduced to $\delta_R = 15$ degrees and then to $\delta_R = 0$ degrees. When the angle of attack has been recovered to about $\alpha = 15$ degrees, a nose-up elevator deflection $\delta_E = -10$ degrees is commanded to slow down the pitch rate. When the angle of attack drops below about $\alpha = 5$ degrees, a nose-down elevator deflection $\delta_E = 6$ degrees is briefly commanded, and then the elevators are returned to trim. The aircraft has been recovered from the deep stall region, and the angle of attack returns to the trim angle of attack of $\alpha = 5$ degrees and the sideslip angle returns to zero degrees. This result is very pleasing, since it shows that the state trajectory and control inputs planned by the optimal trajectory planner agree with a typical prescribed deep stall recovery procedure that would be used by a human pilot.

5. SIMULATION VERIFICATION

The deep stall recovery actions that were planned using the simplified 3DOF model in the previous section will now be applied to the full 6DOF NASA GTM simulation model to verify that the automatic deep stall recovery system can successfully recover the "real" aircraft from deep stall. The simulation results are shown in Fig. 8 and 9. The time histories of the angle of attack, sideslip angle, aileron, elevator, and rudder are shown in Fig. 8. The first part of the simulation from time $t = 0$ to 10 seconds follows exactly the same sequence as was performed in Fig. 4 to push the aircraft into deep stall. However, this time the automatic deep stall recovery system is activated at $t = 10$ seconds. The recovery system captures the aircraft state

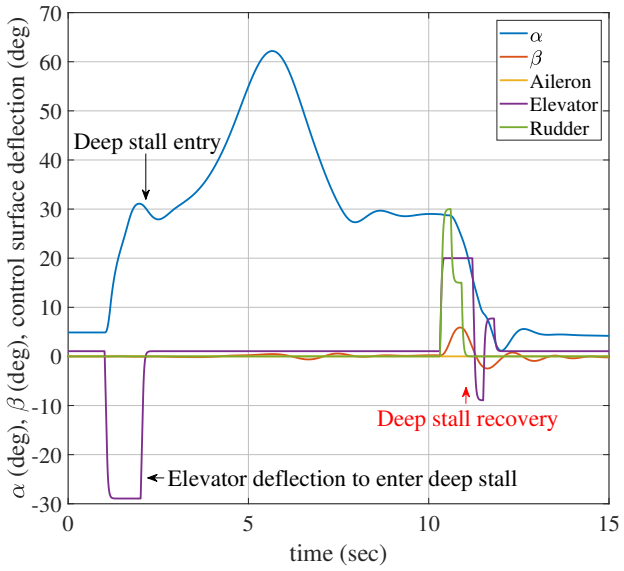

Fig. 8. Simulated deep stall entry and successful recovery

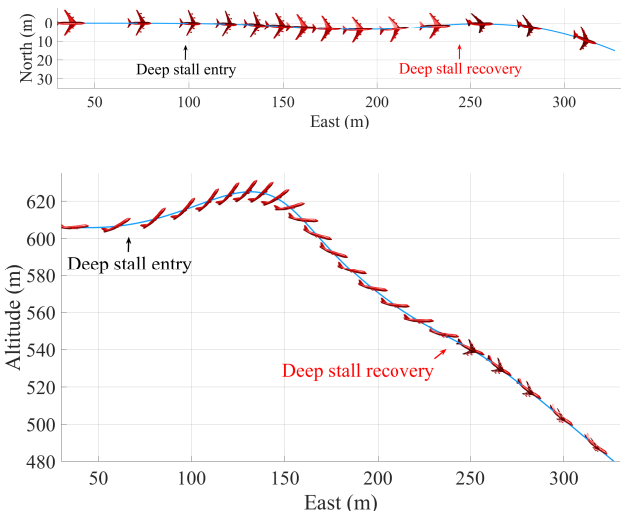

Fig. 9. Deep stall entry and recovery trajectory (top view and side view).

at that moment, plans the optimal sequence of recovery actions, and then executes the planned recovery actions on the aircraft. The simulaton results from time $t = 0$ to 15 seconds show that the full NASA GTM model is successfully recovered from deep stall to the normal aerodynamic envelope following a similar state trajectory to the planned state trajectory that was expected using the simplified 3DOF model. This validates the asssumption that the simplfied 3DOF model can be used to plan the deep stall recovery actions for the full aircraft. After the recovery sequence, the aircraft settles to an angle of attack $\alpha = 6$ degrees and a sideslip angle $\beta = 0$ degrees inside the normal aerodynamic envelope.

The aircraft's trajectory during the deep stall entry and successful automatic recovery is shown in Fig. 9. The trajectory shows that after the deep stall recovery, the aircraft still has a nose-down pitch angle and a steeply descending flight path angle. As mentioned before, the deep stall recovery is only concerned with recovering the aerodynamic envelope, so that the conventional flight control laws and envelope protection functions are available again to perform the next stage of the recovery sequence. Once the aircraft has been recovered from deep stall, a different upset recovery function can be engaged to perform the attitude, flight path angle and airspeed recovery.

REFERENCES

Bunge, R.A. and Kroo, I.M. (2018). Automatic spin recovery with minimal altitude loss. In *AIAA Guidance, Navigation, and Control Conference, 2018*.

Chambers, J. and Grafton, S. (1977). Aerodynamic characteristics of airplanes at high angles of attack. Technical Report NASA TM-74097, NASA.

Cunningham, K., Foster, J., Murch, A., and Morelli, E. (2008). Practical application of a subscale transport aircraft for flight research in control upset and failure conditions. In *Guidance, Navigation, and Control and Co-located Conferences*. American Institute of Aeronautics and Astronautics.

Dutoi, B., Richards, N., Gandhi, N., Ward, D., and Leonard, J. (2008). Hybrid robust control and reinforcement learning for optimal upset recovery. In *Guidance, Navigation, and Control and Co-located Conferences*. American Institute of Aeronautics and Astronautics.

Engelbrecht, J.A.A., Pauck, S.J., and Peddle, I.K. (2012). Bifurcation analysis and simulation of stall and spin recovery for large transport aircraft. In *AIAA Atmospheric Flight Mechanics Conference*.

Engelbrecht, J.A.A., Pauck, S.J., and Peddle, I.K. (2013). A multi-mode upset recovery flight control system for large transport aircraft. In *AIAA Guidance, Navigation, and Control (GNC) Conference*.

Engelbrecht, J.A.A. (2016). *Automatic flight envelope recovery for large transport aircraft*. Ph.D. thesis, Stellenbosch: Stellenbosch University.

Foster, J., Cunningham, K., Fremaux, C., Shah, G., Stewart, E., Rivers, R., Wilborn, J., and Gato, W. (2005). Dynamics modeling and simulation of large transport airplanes in upset conditions. In *Guidance, Navigation, and Control and Co-located Conferences*, m. American Institute of Aeronautics and Astronautics.

Gill, S.J., Lowenberg, M.H., Neild, S.A., Crespo, L.G., Krauskopf, B., and Puyou, G. (2015). Nonlinear dynamics of aircraft controller characteristics outside the standard flight envelope. *Journal of Guidance, Control, and Dynamics*, 38(12), 2301–2308.

Gill, S.J., Lowenberg, M.H., Neild, S.A., Krauskopf, B., Puyou, G., and Coetzee, E. (2013). Upset dynamics of an airliner model: A nonlinear bifurcation analysis. *Journal of Aircraft*, 50(6), 1832–1842.

Hahn, S.H., Hwang, B.M., Lee, Y.H., Lee, D.K., Ahn, S.J., and Kim, C.S. (2007). A study on the design and validation of automatic pitch rocker for the aircraft deep stall recovery. *Journal of Institute of Control, Robotics and Systems*, 13(1), 6–14.

Hueschen, R.M. (2011). Development of the Transport Class Model (TCM) Aircraft Simulation From a Sub-Scale Generic Transport Model (GTM) Simulation. Technical report, NASA.

Kumar, P., Raghavendra, P., Sahai, T., and Ananthkrishnan, N. (2004). Spin recovery of an aircraft using nonlinear dynamic inversion techniques. In *Aerospace Sciences Meetings*. American Institute of Aeronautics and Astronautics.

LaValle, S.M. (2006). *Planning Algorithms*. Cambridge University Press.

Lee, D.C. and Nagati, M.G. (2004). Momentum vector control for spin recovery. *Journal of Aircraft*, 41(6), 1414–1423.

Medina, M. and Shahaf, M. (1990). Post stall characteristics of highly augmented fighter aircraft. In *ICAS, Congress, 17 th, Stockholm, Sweden*, 1976–1983.

Murch, A. and Foster, J. (2007). Recent NASA research on aerodynamic modeling of post-stall and spin dynamics of large transport airplanes. In *Aerospace Sciences Meetings*. American Institute of Aeronautics and Astronautics.

Murch, A.M. (2007). *Aerodynamic modeling of post-stall and spin dynamics of large transport airplanes*. Ph.D. thesis, Georgia Institute of Technology.

Murphy, P. and Klein, V. (2008). Transport aircraft system identification from wind tunnel data. In *Guidance, Navigation, and Control and Co-located Conferences*. American Institute of Aeronautics and Astronautics.

Pauck, S.J. and Engelbrecht, J.A.A. (2012). Bifurcation analysis of the generic transport model with a view to upset recovery. In *AIAA Atmospheric Flight Mechanics Conference*.

Raghavendra, P., Sahai, T., Kumar, P.A., Chauhan, M., and Ananthkrishnan, N. (2005). Aircraft spin recovery, with and without thrust vectoring, using nonlinear dynamic inversion. *Journal of Aircraft*, 42(6), 1492–1503.

Sinha, N.K. and Venkateswara Rao, D.M.K.K. (2010). Aircraft spin recovery using a sliding-mode controller. *Journal of Guidance, Control, and Dynamics*, 33(5), 1675–1679.

Wang, P. and Shi, Z. (2010). Fuzzy recovery controller for deep stall based on particle swarm optimization. *2010 International Conference on Computer Design and Applications, ICCDA 2010*, 3.

Yildiz, A., Akcal, U., Hostas, B., Ure, N.K., and Inalhan, G. (2018). Finite state automata based approach to autonomous stall and upset recovery for agile aircraft. In *2018 AIAA Guidance, Navigation, and Control Conference*. American Institute of Aeronautics and Astronautics.